

promoting access to White Rose research papers



Universities of Leeds, Sheffield and York
<http://eprints.whiterose.ac.uk/>

This is an author produced version of a paper published in ***Journal of the Acoustical Society of America***.

White Rose Research Online URL for this paper:

<http://eprints.whiterose.ac.uk/9167/>

Published paper

Zhang, J., Drinkwater, B.W. and Dwyer-Joyce, R.S. Ultrasonic oil-film thickness measurement: An angular spectrum approach to assess performance limits. *Journal of the Acoustical Society of America*, 2007, **121**(5), 2612-2620.

<http://dx.doi.org/10.1121/1.2713676>

Title:

**Ultrasonic oil-film thickness measurement: an
angular spectrum approach to assess performance
limits**

Authors and Addresses:

Jie Zhang¹, Bruce W. Drinkwater¹ and Rob S. Dwyer-Joyce²

¹Department of Mechanical Engineering, University Walk,

University of Bristol, Bristol BS8 1TR, UK, email: b.drinkwater@bristol.ac.uk

² Department of Mechanical Engineering, Mappin Street,

University of Sheffield, Sheffield S1 3JD, UK

Short Title:

Ultrasonic oil-film thickness measurement

Keywords:

Ultrasound, angular spectrum, reflection coefficient, spring model

Abstract

The performance of ultrasonic oil-film thickness measurement is explored. A ball bearing (type 6016, shaft diameter 80 mm, ball diameter 12.7 mm) is used with a 50 MHz focused ultrasonic transducer mounted on the static shell of the bearing and focused on the oil film. In order to explore the lowest reflection coefficient and hence the thinnest oil-film thickness that the system can measure, three kinds of lubricant oils (Shell T68, VG15 and VG5) with different viscosities were tested. The results show a minimum reflection coefficient of 0.07 for both oil VG15 and VG5 and 0.09 for oil T68. This corresponds to an oil-film thickness of 0.4 μm for T68 oil. An angular spectrum approach is used to analyse the performance of this configuration. The effect of the key measurement parameters (transducer aperture, focal length and centre frequency) is quantified. The simulation shows that for a focused transducer the reflection coefficient tends to a finite value at small oil-film thickness. For the transducer used in this paper the limiting reflection coefficient is shown to be 0.05 and that the oil-film measurement errors increase as the reflection coefficient approaches this value. The implications for improved measurement systems are then discussed.

I. INTRODUCTION

The function of lubricant oil in a machine element such as a bearing is to control friction and wear and hence provide smooth running and a satisfactory life. A large amount of recent lubrication research is devoted to the study, prevention and monitoring of oil degradation [1]. Lubricant degradation in service can lead directly to machine element damage and machinery failure and so on-line monitoring is desirable. The oil-film thickness gives information about the operating condition of the oil and early warning of lubrication failure [2], allowing life prediction or maintenance scheduling.

When an ultrasonic pulse strikes a very thin layer of lubricant (referred to in this paper as the oil-film) in a bearing system, the film behaves mechanically as like a spring [3]. The reflected ultrasonic pulse is then a function of the oil-film stiffness, which in turn depends on the oil-film thickness and its elastic properties. In this way a simple spring-layer model can be used to extract oil-film thickness from the measured reflection coefficient. Dwyer-Joyce *et al.* [3] and Zhang *et al.* [4] used this technique to monitor the oil-film thickness in bearings such as journal bearings, thrust-pad bearings and ball bearings. The results were shown to agree well with models of the bearing performance. The thinnest oil-film thickness measured was about 0.4 μm (corresponding to a reflection coefficient, $R = 0.09$) for Shell T68 engine oil in a 6016 ball bearing system [4]. There is significant interest in measuring even thinner oil-films as much lubrication occurs under boundary lubrication conditions which leads to oil-film thicknesses in the range 1-100 nm [1]. If very low reflection coefficients (which correspond to very thin oil-films) could be measured then this regime could be explored, potentially leading to a range of interesting

measurement devices.

In this paper, the angular spectrum technique is used to analyse the ultrasonic measurement of oil-films. The angular spectrum approach uses a spatial Fourier transform to decompose an arbitrary ultrasonic field into its component plane waves [5]. These plane waves, which propagate at different angles, can then be analysed separately and eventually recomposed into an ultrasonic field by an inverse angular spectrum. The use of the angular spectrum to model the propagation of acoustic fields and the output of transducers has been widely considered [6-10]. A number of authors have also used the angular spectrum approach in conjunction with multi-layered system models. For example Atalar [11] used the angular spectrum method to analyse the performance of acoustic microscopes. He used various simple angular dependent reflection coefficient functions to represent the interaction of the acoustic microscope beam with a surface. Moidu *et al.* [12] used a similar approach to model the inspection of adhesively bonded joints using planar and focused transducers. The adhesive joint was modelled using a spring model of the interface and showed good agreement with a number of normal and oblique incidence experiments. Croce *et al.* [13] extended this analysis by using a full multi-layered system model.

In this paper, the angular spectrum approach is used to model the output from highly focused ultrasonic transducers and the interaction of the resultant acoustic fields with a thin oil-film. The primary aim is to quantify the performance of this measurement system and assess the effect of transducer parameters such as aperture, focal length and centre frequency. Experimentally, a minimum measurable oil-film reflection coefficient was observed and so the secondary aim of this paper is to explain this observation. Throughout the paper the discussion is focused on a specific bearing and

transducer configuration however it should be noted the approach presented is generally applicable.

II. BACKGROUND THEORY

II.A Ball bearing lubrication

For a ball bearing, operating in the elastohydrodynamic (EHD) lubrication regime, the oil-film thickness can be determined numerically from the regression equations of Dowson and Higginson [14]. They showed that the central film thickness, h_c , can be expressed as,

$$\frac{h_c}{R'} = 2.69 \left(\frac{U\eta_0}{E'R'} \right)^{0.67} (\alpha E')^{0.53} \left(\frac{5W}{n_b E' R'^2} \right)^{-0.067} (1 - 0.61e^{-0.73m}) \quad (1)$$

where, U is the mean surface speed, η_0 is the lubricant viscosity at the contact entry, and α is the pressure-viscosity coefficient, W is the radial load on the whole bearing and n_b is the number of balls, m is the ellipticity parameter, E' is the reduced elastic modulus and R' is the reduced radius of curvature given by,

$$\frac{1}{E'} = \frac{1}{2} \left[\frac{1-\nu_a^2}{E_a} + \frac{1-\nu_b^2}{E_b} \right], \quad \frac{1}{R'} = \frac{1}{R_{ax}} + \frac{1}{R_{bx}} + \frac{1}{R_{ay}} + \frac{1}{R_{by}} \quad (2)$$

where E is Young's modulus, ν is Poisson's ratio. As shown in figure 1, the subscripts a and b refer to the two rolling elements (i.e. the ball and the raceway) and x and y refer to the co-ordinate axes. The contact area is elliptical in shape with the major (r_a) and minor (r_b) semi-contact radii given by,

$$r_a = \left(\frac{30m^2 nWR'}{n_b \pi E'} \right)^{1/3}, \quad r_b = \left(\frac{30nWR'}{n_b \pi m E'} \right)^{1/3} \quad (3)$$

where n is a measure of the shape of the contact ellipse. In this paper a 6016 ball bearing was used and the parameters used in equations 1-3 are given in table 1 and the properties of the three oils used (T68, VG15, VG5) are shown in table 2. Note that the properties at 1.5 GPa are extremely difficult to measure and so are only accurately available for T68 oil [15].

II.B Reflection coefficient from an oil-film

Figure 2 shows a solid-lubricant layer-solid system, which represents the 3-layer structure of a rolling element bearing. Surface 1 and 2 represent the bearing raceway surface and ball surface, respectively. When an ultrasonic plane wave propagates through this structure, ultrasound will be reflected from both the top and bottom surfaces of the oil-film. However, as the oil-film is small compared to the wavelength it is modelled as a boundary condition between the raceway and ball [16]. The lubricant layer is then described by its normal and tangential stiffness, denoted by K_N and K_T respectively. The normal stiffness of the lubricant layer can be simply related to its thickness, h , and bulk modulus, B (where $B = \rho_f c_f^2$ and ρ_f is the density of the lubricant layer and c_f is the velocity of the longitudinal wave in the lubricant layer) by [3],

$$K_N = \frac{B}{h} \quad (4)$$

Figure 2 also shows the various waves which could exist where A is the amplitude of the plane wave, subscripts l and s refer to the longitudinal wave and shear wave

respectively, and superscripts 1 and 2 represent the media. Of particular interest to this paper are $A^{1(l+)}$, the incident longitudinal wave in medium 1 and $A^{1(l-)}$ the reflected longitudinal wave in medium 1. In this notation the longitudinal wave reflection coefficient in medium 1 is given by,

$$R(\omega, \theta) = \frac{A^{1(l-)}}{A^{1(l+)}} \quad (5)$$

Assuming that the solid half-spaces either side of the lubricant layer have identical acoustic properties the amplitudes of the various plane waves are related by [16-18],

$$\begin{Bmatrix} A^{2(l+)} \\ A^{2(l-)} \\ A^{2(s+)} \\ A^{2(s-)} \end{Bmatrix} = [D]^{-1} [S] [D] \begin{Bmatrix} A^{1(l+)} \\ A^{1(l-)} \\ A^{1(s+)} \\ A^{1(s-)} \end{Bmatrix} \quad (6)$$

where, $[D]$ defines the relationship between the wave amplitudes and the normal and shear stresses and displacements and $[S]$ describes the spring boundary condition between the two media. Matrices $[D]$ and $[S]$ are given by,

$$[D] = \begin{bmatrix} c_l C_i C_{2\beta} & c_l C_i C_{2\beta} & -2s c_s^2 C_i C_2 & 2s c_s^2 C_i C_2 \\ 2s c_s^2 C_i C_1 & -2s c_s^2 C_i C_1 & c_s C_i C_{2\beta} & c_s C_i C_{2\beta} \\ c_l s & c_l s & C_2 & -C_2 \\ C_1 & -C_1 & -c_s s & -c_s s \end{bmatrix} \quad (7)$$

$$[S] = \begin{bmatrix} 1 & 0 & 0 & 0 \\ 0 & 1 & 0 & 0 \\ 0 & \frac{1}{K_T} & 1 & 0 \\ \frac{1}{K_N} & 0 & 0 & 1 \end{bmatrix} \quad (8)$$

where $C_1 = (1 - c_l^2 s^2)^{\frac{1}{2}}$, $C_2 = (1 - c_s^2 s^2)^{\frac{1}{2}}$, $C_{2\beta} = 1 - 2c_s^2 s^2$, $C_i = i\omega\rho$,
 $s = \frac{\sin(\theta_l)}{c_l} = \frac{\sin(\theta_s)}{c_s}$, ω is the centre frequency of the plane wave and θ is its incident angle, defined with respect to the surface normal.

Note that for the case of a longitudinal wave, normally incident on a lubricant layer, equations 4-8 can be simplified to calculate film thickness as [3],

$$h = \frac{2B}{\omega Z} \sqrt{\frac{|R_n(\omega)|^2}{1 - |R_n(\omega)|^2}} \quad (9)$$

where, Z is the acoustic impedance of the media surrounding the lubricant film and $R_n(\omega)$ is the amplitude of the normal incident plane wave reflection coefficient.

III. BALL BEARING EXPERIMENTAL APPARATUS

Figure 3(a) shows the experimental apparatus used to measure the ultrasonic reflection coefficient from an oil-film in a 6016 ball bearing system. A rotating shaft of 80 mm diameter was supported on four 6016 ball bearings lubricated via a total loss gravity feed system. Bearings 1 and 4 were fitted to the ends of the shaft and fixed into rigid housings. Vertically upwards radial loads were applied to the central region of the shaft through bearings 2 and 3 via an arrangement of springs. This meant that in bearings 1 and 4 the balls at the top of the raceway were the most heavily loaded. The rotary shaft speed was controllable in the range 100-2900 rpm by a 7.5 kWatt electric motor. This control of load and speed then enabled control of the resultant oil-film thickness via equation 1.

An optical sensor was used, both to allow accurate triggering of the ultrasonic instrumentation and to measure shaft speed. This was triggered by reflective tape attached to the ball cage (which rotates at half the shaft speed). Bearing 1 was instrumented with the ultrasonic measurement system that is shown in figure 3(b). A focused, longitudinal wave piezoelectric ultrasonic transducer was mounted in the housing such that it was normal to the top surface of the outer raceway. This transducer acted as both an emitter and receiver (pulse-echo mode), and its parameters show in table 3. The transducer was focused on the outer raceway (4.5 mm thickness) and designed to achieve a focal zone size smaller than the width of the lubricated contact region. An ultrasonic pulser-receiver (Panametrics 5072PR) was used to excite the ultrasonic transducer, receive and amplify the reflected signals which were then passed to a digital scope (sampling frequency 5 GHz) and PC for storage and analysis.

The reflective tape attached to the bearing cage is also shown in figure 3(b). When this tape passed the optical sensor it generated a 5V positive trigger pulse. This pulse was used to trigger a signal generator (Agilent 33220A). After the addition of an adjustable delay the signal generator then triggered the pulser-receiver at its maximum pulse repetition frequency, which was 20 kHz. By triggering in this way, a number of ultrasonic pulses were able to interrogate the lubricated contact region as it passed under the transducer.

The reflection coefficient was measured by comparing the signal reflected from the oil-film, $A_m(\omega)$, with that from a reference interface, $A_{ref}(\omega)$,

$$R(\omega) = \frac{A_m(\omega)}{A_{ref}(\omega)} R_{ref}(\omega) \quad (10)$$

where, $R_{ref}(\omega)$ is the reflection coefficient of the reference interface, which in this case was a steel-air interface obtained before the lubricant was introduced. This reflection coefficient was then used in equation 9 to obtain the oil-film thickness.

Three oils with different viscosities (Shell T68, VG15, VG5) were used to explore the minimum measurable oil-film thickness. In general, oils with lower viscosities generate thinner oil-films for the same operating conditions (i.e. bearing load and speed). For this reason it was thought that the lowest reflection coefficient would result from the lowest viscosity oil.

IV. RESULTS

Figure 4 shows measurements of reflection coefficient for the three oils (Shell T68, VG15, VG5) for a range of different operating speeds (ω) and loads (W). From figure 4 it can be seen that the reflection coefficient decreases with increased load for all oils. It can also be seen that for a given oil the reflection coefficient decreases as speed decreases and that the lower viscosity oils exhibit lower reflection coefficients. Qualitatively, all these trends follow the changes in oil-film thickness predicted by equation 1, bearing in mind that a lower oil-film thickness is the cause of a lower reflection coefficient. However, it can also be seen that the reflection coefficients appear to reach a limiting value (of approximately 0.07) rather than tending to zero at high load and low speed as equation 1 would suggest.

V. DISCUSSION

This section considers the effect of the transducer parameters such as aperture, D , focal length, F , and centre frequency, f_c , on oil-film thickness measurement by using the angular spectrum approach. The spring-layer model (i.e. equations 5-8) is used to model the wave interactions with the oil-film.

V.A Angular spectrum approach

The geometry of the measurement system used for the modelling is shown in figure 5. For simplicity, the transducer is modelled as if it were directly coupled to the steel of the bearing shell. This modelled transducer is then forced to focus on the lubricated raceway-ball interface and so the need to model the propagation in the water is removed. The aperture size is adjusted by a simple trigonometric calculation to account for the small focussing effect in the water. In this way the 6.25 mm diameter transducer with a focal length of 23 mm in water used experimentally (see table 3) becomes a 5 mm diameter transducer of focal length in steel of 4.5 mm in direct contact with the steel (see table 3). In figure 5, the planes labelled 1 and 2 represent the modelled transducer plane and focal plane respectively and plane 2 is also the plane of the oil-film. In the discussion that follows, the superscripts + and – refer to fields propagating in the + z and – z directions, respectively.

The axial pressure of a focused circular transducer is given by [19] as,

$$p = \left| \frac{2}{1 - \frac{z}{a}} \right| \left| \sin \left[\frac{\pi}{\lambda} \left(\sqrt{\left(z - a + \sqrt{a^2 - \frac{D^2}{4}} \right)^2 + \frac{D^2}{4}} - z \right) \right] \right| \quad (11)$$

where, λ is the wavelength, a is the radius of curvature of the transducer, D is the aperture of the transducer, and $a > D/2$ is assumed. If the focal length, F , defined as

the distance at which pressure is a maximum then this equation can then used to calculate the effective radius of curvature which results in the desired focal length (i.e. 4.5 mm in this case and equal to the bearing raceway thickness in general).

The displacement field at plane 1 due to the transducer is then modelled by the following two dimensional windowing function,

$$u_1^+(x, y) = \begin{cases} 1 & \text{when } \sqrt{x^2 + y^2} \leq \beta \frac{D}{2} \\ 0.5 \times \left[\cos\left(\frac{\pi \sqrt{x^2 + y^2}}{D/2}\right) + 1 \right] & \beta \frac{D}{2} < \sqrt{x^2 + y^2} < \frac{D}{2} \\ 0 & \sqrt{x^2 + y^2} \geq \beta \frac{D}{2} \end{cases} \quad (12)$$

where the coefficient β defines the extent of the piston-like region of the transducer (in this paper $\beta=0.9$). This taper was used to better represent a real transducer as well as reducing the amplitude of the high spatial frequency components that result from the use of a pure piston source (which is essentially a rectangular windowing function). Following the approach of [6] the angular spectrum at plane 1 $U_1^+(k_x, k_y)$ is obtained by taking a spatial Fourier transform (denoted by FT) of the displacement field,

$$U_1^+(k_x, k_y) = \text{FT}(u_1^+(x_1, y_1)) = \int_{-\infty}^{+\infty} \int_{-\infty}^{+\infty} u_1^+(x_1, y_1) \cdot \exp(-j(k_x x_1 + k_y y_1)) dx_1 dy_1 \quad (13)$$

where k_x and k_y are the wavenumbers in the x and y directions respectively. In practice equation 13 is implemented using a Fast Fourier Transform (FFT) routine on an array of data representing the discretised spatial distribution of displacements. Equation 13 is then multiplied by a phase term to account for propagation from plane

1 to plane 2 (i.e. the focal plane),

$$U_2^+(k_x, k_y) = U_1^+(k_x, k_y) \cdot \exp\left(-j\left(\sqrt{k_0^2 - \sqrt{k_x^2 + k_y^2}}\right)F\right) \quad (14)$$

where k_0 is the wavenumber in the steel and $k_0 = \frac{\omega}{c_{steel}}$. If it is assumed that all the reflected ultrasound comes from the lubricated contact region then the reflected field can be found from [6 and 12],

$$U_2^-(k_x, k_y) = U_2^+(k_x, k_y) \cdot R(\omega, \theta) \quad (15)$$

where, from equation 5, $R(\omega, \theta)$ is the oil-film reflection coefficient for a plane wave

at an angle, θ , with respect to the normal of plane 2, $\theta = \sin^{-1}\left(\frac{\sqrt{k_x^2 + k_y^2}}{k_0}\right)$. A further

identical propagation term can then be used to simulate the propagation in the $-z$ direction back to plane 1 to give,

$$U_1^-(k_x, k_y) = U_1^+(k_x, k_y) \cdot \exp\left(-j \cdot 2\left(\sqrt{k_0^2 - \sqrt{k_x^2 + k_y^2}}\right)F\right) \cdot R(\omega, \theta) \quad (16)$$

The acoustic field reflected back to plane 1 and hence received by the transducer is then found by an inverse spatial FT of $U_1^-(k_x, k_y)$,

$$u_1^-(x, y) = \text{FT}^{-1}\left(U_1^-(k_x, k_y)\right) = \frac{1}{4\pi^2} \int_{-\infty}^{+\infty} \int_{-\infty}^{+\infty} U_1^-(k_x, k_y) \cdot \exp(j(k_x x_1 + k_y y_1)) dx_1 dy_1 \quad (17)$$

The amplitude recorded by the transducer, A , can then be calculated as the weighted sum of $u_1^-(x, y)$ over the transducer surface where the weighting function is that of the

original transducer output, i.e. equation 12.

$$A = \sum_{x^2+y^2 < (D/2)^2} u_1^-(x, y) \cdot u_1^+(x, y) \quad (18)$$

Figure 6 shows a simulation of the measurement system obtained using this approach. The acoustic properties of the media and transducer characteristics used in the simulation are shown in table 2 and 3 respectively. A source plane (50×50 mm) was defined with a spatial sampling interval of 25 μm (i.e. Δx=Δy=25 μm). Figure 6(a) shows the amplitude distribution at the focal plane (i.e. plane 2) obtained by equation 14 as well as the size of the lubricated contact region in a 6016 ball bearing for a 15 kN radial load from equation 3. From figure 6(a), it can be seen that the assumption that the majority of the acoustic field is within the contact ellipse is reasonable. Figure 6(b) shows the predicted reflection coefficient distribution and weighted sum reflection coefficient for various oil-films. To generate this figure equations 17 and 18 were used to calculate the displacement distribution and weighted sum at the transducer. Simulations were performed for both the thin-film case and the reference case (i.e. steel-air) and used in equation 10 to compute reflection coefficient (using $R_{ref}=1.0000$). For the reflection coefficient distribution, equation 10 was performed for each spatial point. In this way the model replicated the experimental procedure. From figure 6(b) it can be seen that as the thickness of the oil-film increases, so the reflection coefficient distribution becomes flatter and begins to approach that of the weighted sum. It can also be seen from figure 6(b) that as the oil-film thickness decreases so the acoustic field distribution (and hence the sum) approach plateau values. For example, oil-films of thickness 0.001 μm and 0.0001 μm can be seen to have barely distinguishable reflection coefficients. This

suggests that, for the particular transducer modelled there is a finite limiting reflection coefficient below which measurement is not possible. This in turn implies a limiting thickness as was observed experimentally in figure 4.

Simulations were performed for a range of oil-film thicknesses, and the weighted sum reflection coefficient shown in figure 7(a), with a zoom of the important low thickness region shown in figure 7(b). Also shown in these figures is the normal incidence reflection coefficient (R_n) as a function of oil-film thickness. As the transducer is mounted at normal incidence it would be standard practice to use the normal incidence relationship to compute the oil-film thickness. For this reason the relative difference between the reflection coefficient measured by a focused transducer and the normal incidence plane wave reflection coefficient is defined as,

$$\varepsilon = \left| \frac{h(R_{wei}) - h(R_n)}{h(R_n)} \right| \times 100\% \quad (19)$$

where, $h(R)$ is the oil-film thickness obtained from equation 9, the normal incidence spring model. From figure 7(b) it can be seen that the smallest measurable reflection coefficient (labelled " R_{lim} ") for the simulated transducer is 0.05. Figure 7(c) shows the relationship between the weighted sum reflection coefficient (R_{wei}) and the normal incident reflection coefficient (R_n) (labelled "calibration line"). As the calibration line departs from a line of unity gradient and zero intercept so the error between the normal incidence plane wave and the focused transducer reflection coefficient increases. For example, it can be seen from figure 7(c) that for a reflection coefficient of 0.1 measured with the focused transducer, the resultant oil-film thickness measurement error obtained from equation 9 is $\varepsilon = 17\%$. In principle, the calibration

line shown in figure 7(c) could be used to compensate for this difference. As can be seen from table 4 a reflection coefficient of 0.09 was measured for T68 oil at 15 kN and 106 rpm and this corresponds to a 0.41 μm oil-film thickness. If the calibration line in figure 7(c) is used to compensate for the focusing effect then the “effective” normal incidence reflection coefficient becomes 0.07, which corresponds to a 0.31 μm oil-film thickness. Note that in this case the EHD model value obtained from equation 1 is $h_c=0.27 \mu\text{m}$. Similar results are shown in table 4 for the other oils. The VG5 oil has the lowest viscosity of the three oils tested and so resulted in the thinnest oil films (and therefore the lowest reflection coefficients). The calibration approach described above has then been applied to the measured reflection coefficient data for this oil and the result is shown in figure 4. For example from table 4 it can be seen that at 15 kN and 106 rpm a reflection coefficient of 0.07 was measured which, after calibration becomes 0.05. Although the acoustic properties of the VG5 oil under high pressures are not accurately known, if a similar relationship between pressure, density and bulk modulus is assumed then this minimum reflection coefficient equates to $h_c=0.2 \mu\text{m}$. This is therefore the thinnest oil-film yet measured using ultrasound and this approach suggests a possible way forward to measure even thinner films. The transducer parameters responsible for the effects described in this section are now considered in more detail. In particular, experimental configurations which would enable the measurement of even thinner films are considered.

V.B Variation of transducer parameters

For a transducer with $F=4.5 \text{ mm}$ and $f_c=50 \text{ MHz}$, figure 8 shows the limiting reflection coefficient, R_{lim} , and the reflection coefficients which result in various

levels of oil-film thickness error, R_ε ($\varepsilon = 2\%$, 5% , 10%) as a function of transducer aperture. From figure 8, it can be seen that both R_{lim} and R_ε increase with transducer aperture, D . This is because a focused transducer with a large aperture size can be thought of as emitting plane waves over a wide range of angles. Some of these plane waves are then obliquely incident on the oil-film and are hence sensitive to a different reflection coefficient than the normal incident plane waves. This implies that for oil-film thickness measurement, the smaller aperture of the transducer, the better the measurement. However, the aperture must be such that the focal zone size is smaller than the lubricated contact.

For a given transducer aperture, $D=5$ mm and $f_c=50$ MHz, figure 9 again shows R_{lim} and R_ε for various error cases ($\varepsilon = 2\%$, 5% , 10%), this time as a function of focal length. From figure 9, it can be seen that both R_{lim} and R_ε decrease as the focal length increases. As for the aperture the reason for this effect is that a focused transducer with a long focal length emits plane waves over a smaller range of angles. This implies that a large focal length is beneficial however, at 50 MHz the requirement for a small focal zone size forces the choice of a focal length to be as small as possible and hence equal to the bearing thickness.

For a given $F=4.5$ mm and $D=5$ mm, figure 10 shows R_{lim} and R_ε for various error cases ($\varepsilon = 2\%$, 5% , 10%) as function of centre frequency. From figure 10, it can be seen that R_{lim} is almost constant (0.05). However it should be noted that according to the spring-layer model (equation 9), a given reflection coefficient corresponds a smaller oil-film thickness at a higher frequency. Hence, the smallest measurable oil-film thickness hence decreases with increased frequency.

From the analysis in this section, it can be seen that the ideal transducer for oil-film thickness measurement would have a high centre frequency, a small aperture size and long focal length. Figure 11 shows the performance of a possible transducer with these features i.e. $f_c=150$ MHz, $D=1$ mm and $F=4.5$ mm focal length. From this figure it can be seen that it is possible to measure a reflection coefficient of 0.08 with 2% error. This corresponds to a $0.12\ \mu\text{m}$ oil-film thickness for T68 oil in a 6016 bearing at 15 kN and 106 rpm.

VI. CONCLUSIONS

The use of a focused transducer to measure oil-film thickness has been shown to generate errors if not approached with care. These errors increase as oil film thickness decreases, potentially limiting the ability of ultrasound to measure very thin oil-films. The angular spectrum approach has been used to model the measurement system and the interaction of the resultant plane waves with a spring-layer. The analysis showed that oil-film thickness measurement errors decrease as centre frequency and focal length increase and transducer aperture decreases. For a specific focused transducer (50 MHz centre frequency, focal length of 4.5 mm and aperture of 5 mm) the theoretical thickness measurement error was predicted to be 17% when the measured reflection coefficient was 0.1, and a finite reflection coefficient limit was reached at 0.05. This compared well with the experimentally observed reflection coefficient limit of 0.07. A calibration approach was described which allowed an oil-film thickness of $0.2\ \mu\text{m}$ to be measured, thinner than had previously been possible. For the T68 oil which has well known acoustic characteristics the experimental results were shown to be in improved agreement with known lubrication theory after calibration. The use of a small, high frequency transducer was then shown to offer

improved performance on very thin oil-films.

ACKNOWLEDGEMENTS

This work has been funded by the UK Engineering and Physical Sciences Research Council under Grant No. GR/S046956/01.

REFERENCES

1. G.W. Stachowiak and A.W. Batchelor, *Engineering Tribology* (Butterworth Heinemann, Woburn, MA, 2001).
2. J. Zhang, B.W. Drinkwater and R.S. Dwyer-Joyce, "Monitoring of lubricant film failure in a ball bearing using ultrasound," *J. Tribol.-Trans. ASME* **128**, 622-618 (2006).
3. R.S. Dwyer-Joyce, B.W. Drinkwater and C.J. Donohoe, "The measurement of lubricant-film thickness using ultrasound," *Proc. R. Soc. Lond. A.* **459**, 957-976 (2003).
4. J. Zhang, B.W. Drinkwater and R.S. Dwyer-Joyce, "The measurement of lubricant-film thickness in rolling element bearings using ultrasound," *J. Acoust. Soc. Am.* **119**, 863-871 (2006).
5. J.W. Goodman, *Introduction to Fourier optics*, (McGraw Hill, New York, 1978).
6. P.R. Stepanishen and K.C. Benjamin, "Forward and backward projection of acoustic fields using FFT methods," *J. Acoust. Soc. Am.* **71**, 803-812 (1994).
7. P.T. Christopher and K.J. Parker, "New approaches to the linear propagation of

- acoustic fields,” J. Acoust. Soc. Am. **90**, 507-521 (1991).
8. D.P. Orofino and P.C. Pedersen, “Efficient angular spectrum decomposition of acoustic sources – part I: theory,” IEEE Trans. Ultrason. Ferr. Freq. Cont. **40**, 238-249 (1993).
9. C.J. Vecchio and P.A. Lewin, “Finite amplitude acoustic propagation modelling using the extended angular spectrum method,” J. Acoust. Soc. Am. **94**, 2399-2408 (1994).
10. P. Wu, R. Kazys and T. Stepinski, “Optimal selection of parameters for the angular spectrum approach to numerically evaluate acoustic fields,” J. Acoust. Soc. Am. **101**, 125-134 (1997).
11. A. Atalar, “An angular-spectrum approach to contrast in reflection acoustic microscopy,” J. Appl. Phys. **49**, 5130-5139 (1978).
12. A.K. Moidu, A.N. Sinclair and J.K. Spelt, “Nondestructive characterization of adhesive joint durability using ultrasonic reflection measurements,” Res. Nondestr. Eval. **11**, 81-95 (1999).
13. R. Croce, P. Calmon and L. Paradis, “Modeling of propagation and echo formation in a multilayered structure,” Ultrasonics **38**, 537-541 (2000).
14. D. Dowson and G.R. Higginson, *Elasto-Hydrodynamic Lubrication* (Pergamon Press, New York, 1977).
15. O.B. Jacobson and A.P. Vinet, “Model for the influence of pressure on the bulk modulus and the influence of temperature on the solidification pressure for liquid

lubricants,” J. Tribol.-Trans. ASME **109**, 709-714 (1987).

16. T.P. Pialucha and P. Cawley, “The detection of thin embedded layers using normal incidence ultrasound,” *Ultrasonics* **32**, 431-440 (1994).

17. M.J.S. Lowe, “Matrix techniques for modelling ultrasonic waves in multilayered media,” *IEEE Trans. Ultrason. Ferr. Freq. Cont.* **42**, 525-542 (1995).

18. S.I. Rokhlin and Y.J. Wang, “Analysis of boundary conditions for elastic wave interaction with an interface between two solids,” *J. Acoust. Soc. Am.* **89**, 503-515 (1990).

19. H.T. O’Neil, “Theory of focusing radiators,” *J. Acoust. Soc. Am.* **21**, 516-526 (1949).

Tables

Table 1. Parameters used to calculate the theoretical oil-film thickness in a 6016 ball bearing via equation 1 [14].

Reduced modulus E' (GPa)	Reduced radius R' (m)	Pressure viscosity coefficient for T68 α (Gpa ⁻¹)	Ellipticity parameter m	Simplified Elliptical Integrals n	Effective viscosity for T68 η_0 (N/m ² s)
228	5.85e-3	20	11.5	1.014	0.2

Table 2. Acoustic properties of lubricant oils and steel.

	Effective viscosity η_0 (N/m ² s)	Density ρ (kg/m ³)	Longitudinal wave velocity c_l (m/s)	Bulk modulus B (Gpa)
T68 at 0.1 Mpa	0.2	876	1460	1.84
T68 at 1.5 Gpa	0.2	1044	4500	21.2
VG15 at 0.1 Mpa	0.07	940	1470	2.03
VG5 at 0.1 Mpa	0.03	980	1480	2.14
Steel (EN24)	-	7900	5900	172

Table 3. Experimental and modelled transducer parameters.

	Centre frequency f_c (MHz)	Focal length F (mm)	Active element diameter D (mm)	Taper window coefficient β
Experiment	50	23 (in water)	6.35	n/a
Model	50	4.5 (in steel)	5	0.9

Table 4. Reflection coefficient and oil-film thicknesses for various oils and operating conditions. Also shown are oil-film thickness values from EHD theory [14].

		T68	VG15	VG5
$w=106$ rpm, $L=15$ kN	R (Meas)	0.09	0.07	0.068
	h_c (μm)	0.41	0.31	0.3
	R (Calib)	0.07	0.05	0.046
	h_c (μm)	0.31	0.22	0.2
	EDH Theory h_c (μm)	0.27	0.14	0.07
$w=506$ rpm, $L=15$ kN	R (Meas)	0.18	0.112	0.11
	h_c (μm)	0.81	0.5	0.49
	R (Calib)	0.177	0.099	0.097
	h_c (μm)	0.8	0.44	0.43
	EDH Theory h_c (μm)	0.78	0.40	0.23

List of Figures

Figure 1. Geometry of the contact between the outer-raceway of the bearing and ball.

Figure 2. Three-layer system model of the oil-film.

Figure 3. (a) Schematic diagram of the experimental apparatus made up of four 6016 ball bearings, (b) Transducer attachment and bearing geometry.

Figure 4. Experimentally measured reflection coefficients for three oils (T68, VG15 and VG5) at various operating condition Also shown is the calibrated reflection coefficient for oil VG5.

Figure 5. Geometry of the focused transducer used for the angular spectrum simulation.

Figure 6. Simulation results for the modelled transducer (defined in table 3). (a) Amplitude distribution at the focal plane. (b) Reflection coefficient distribution along the x-axis for a number of oil-film thicknesses.

Figure 7. Simulated reflection coefficient results from a range of oil-film thicknesses by using the modelled transducer (defined in table 3). (a) Reflection coefficients as a function of oil-film thickness. (b) Zoom in the left corner area in Figure 7(a). (c) Calibration line.

Figure 8. Reflection coefficient as a function of transducer aperture, $F=4.5$ mm and $f_c=50$ MHz are assumed.

Figure 9. Reflection coefficient as a function of focal length of the transducer,

$D=5$ mm and $f_c=50$ MHz are assumed.

Figure 10. Reflection coefficient as a function of centre frequency of the transducer,

$F=4.5$ mm and $D=5$ mm are assumed.

Figure 11. Theoretical error from a focused transducer with 1 mm aperture, 150 MHz center frequency and 4.5 mm focal length.

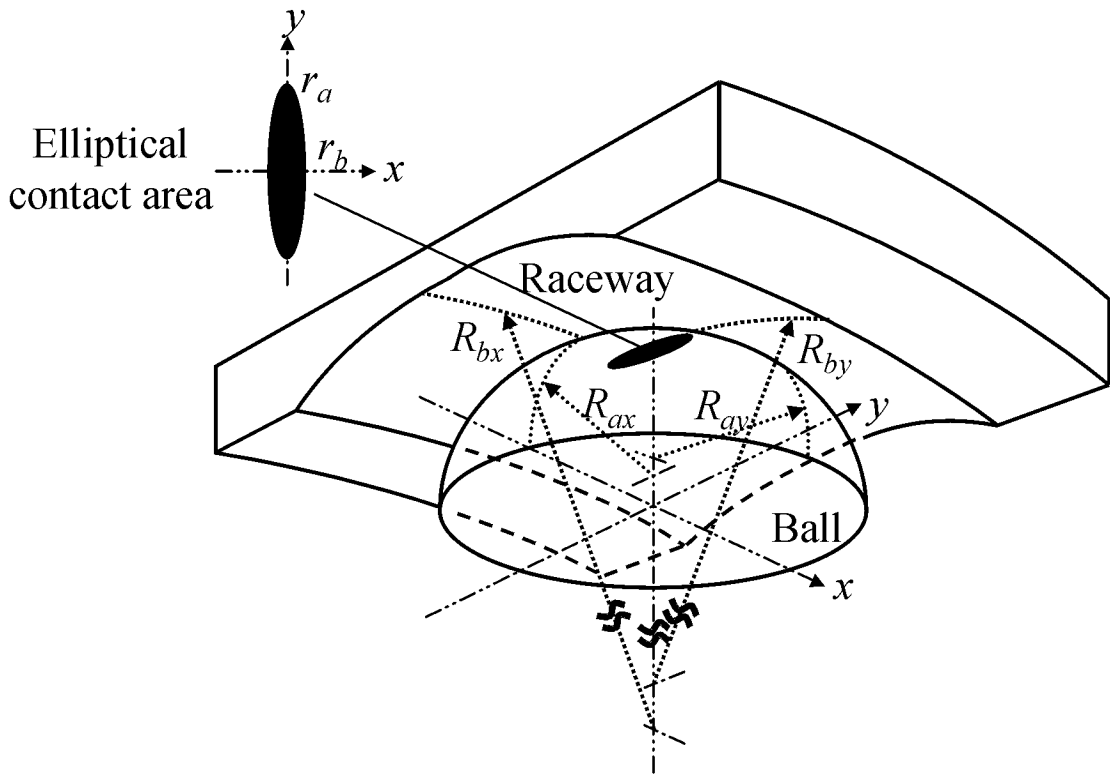


Figure 1.

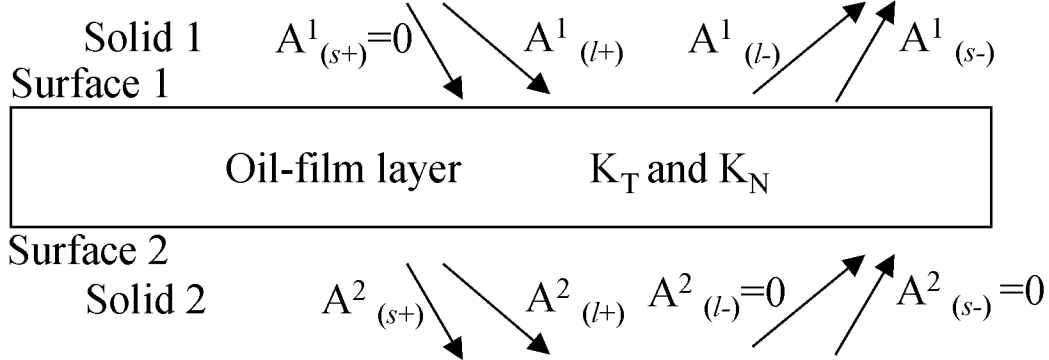


Figure 2.

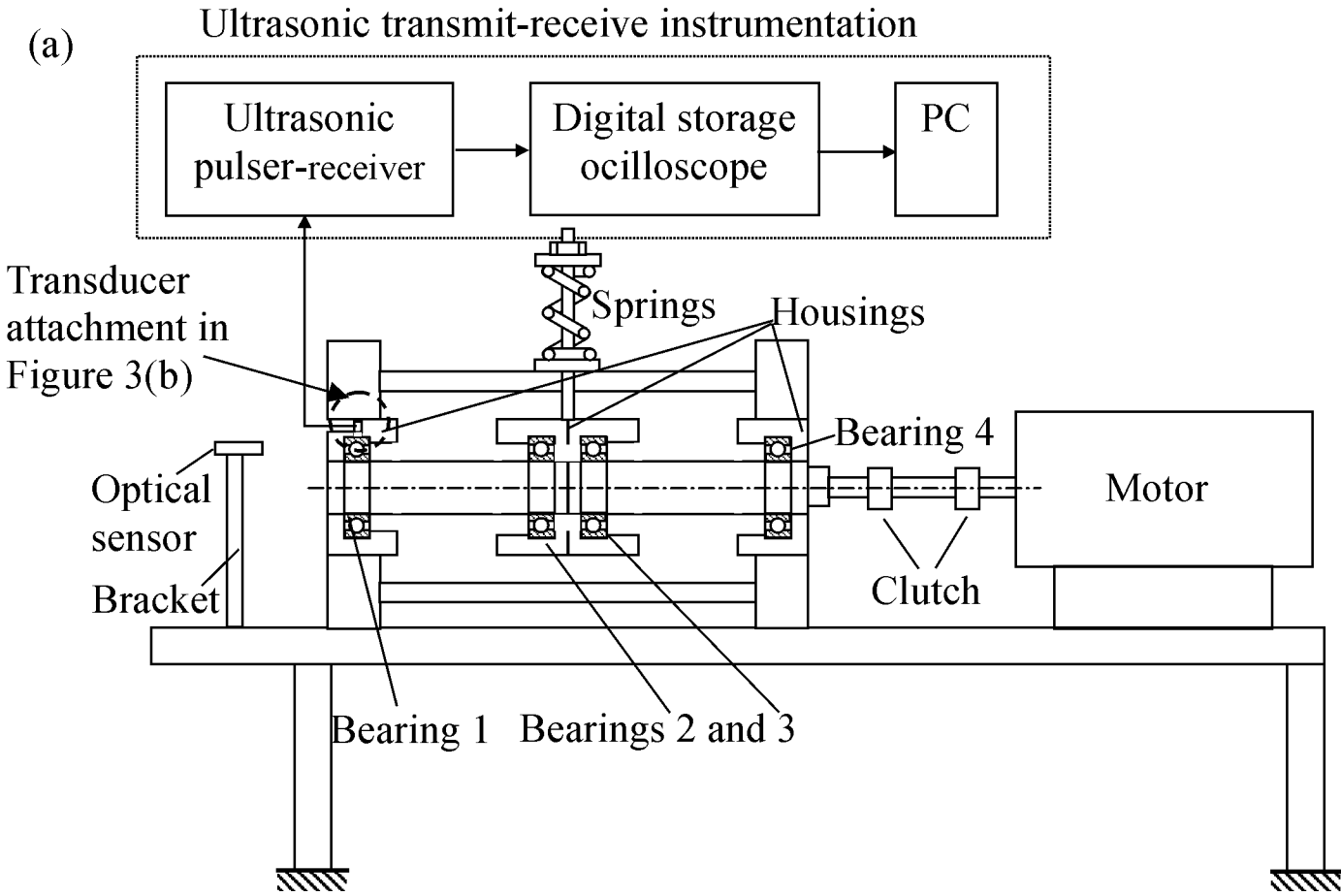


Figure 3(a).

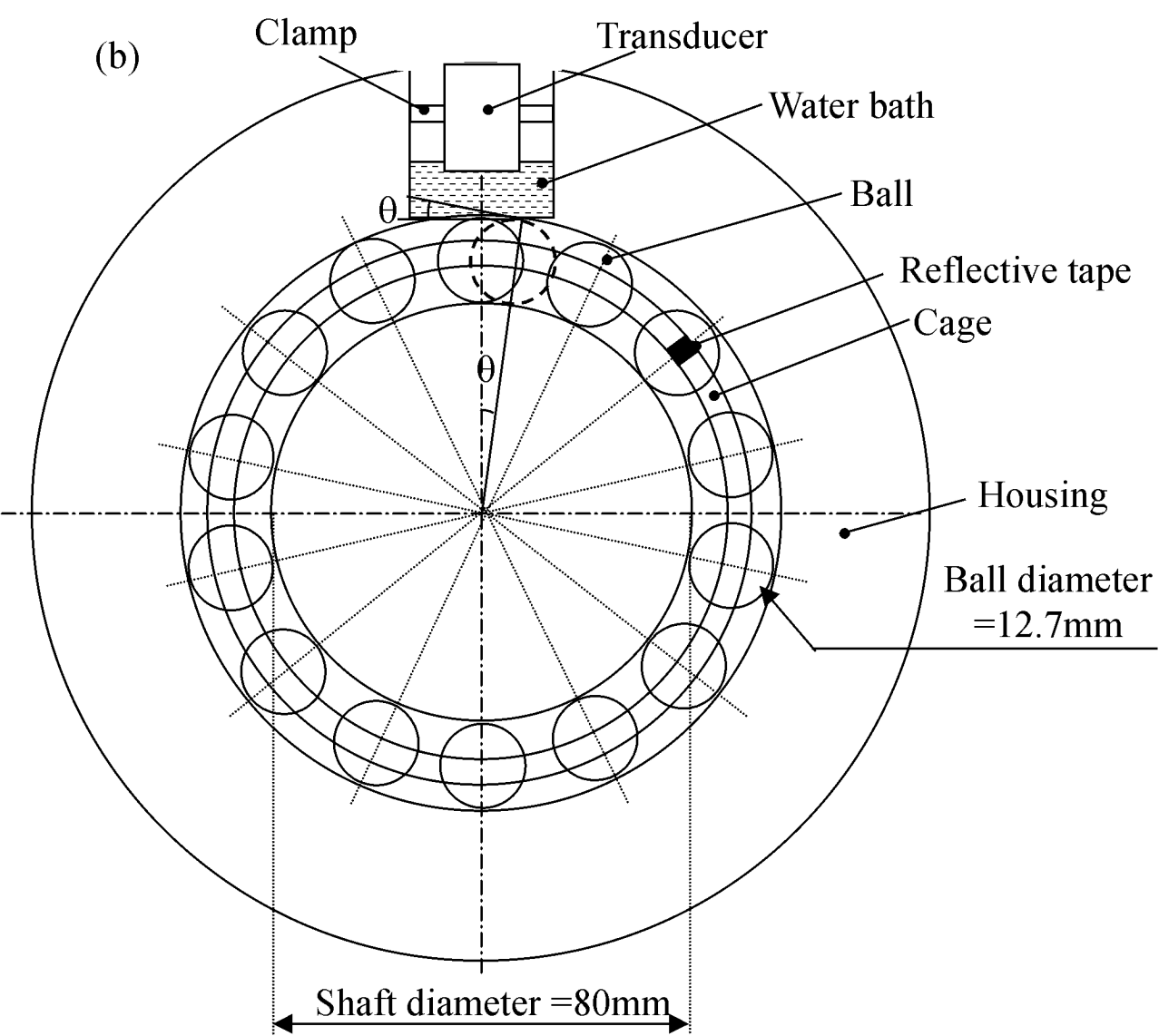


Figure 3(b).

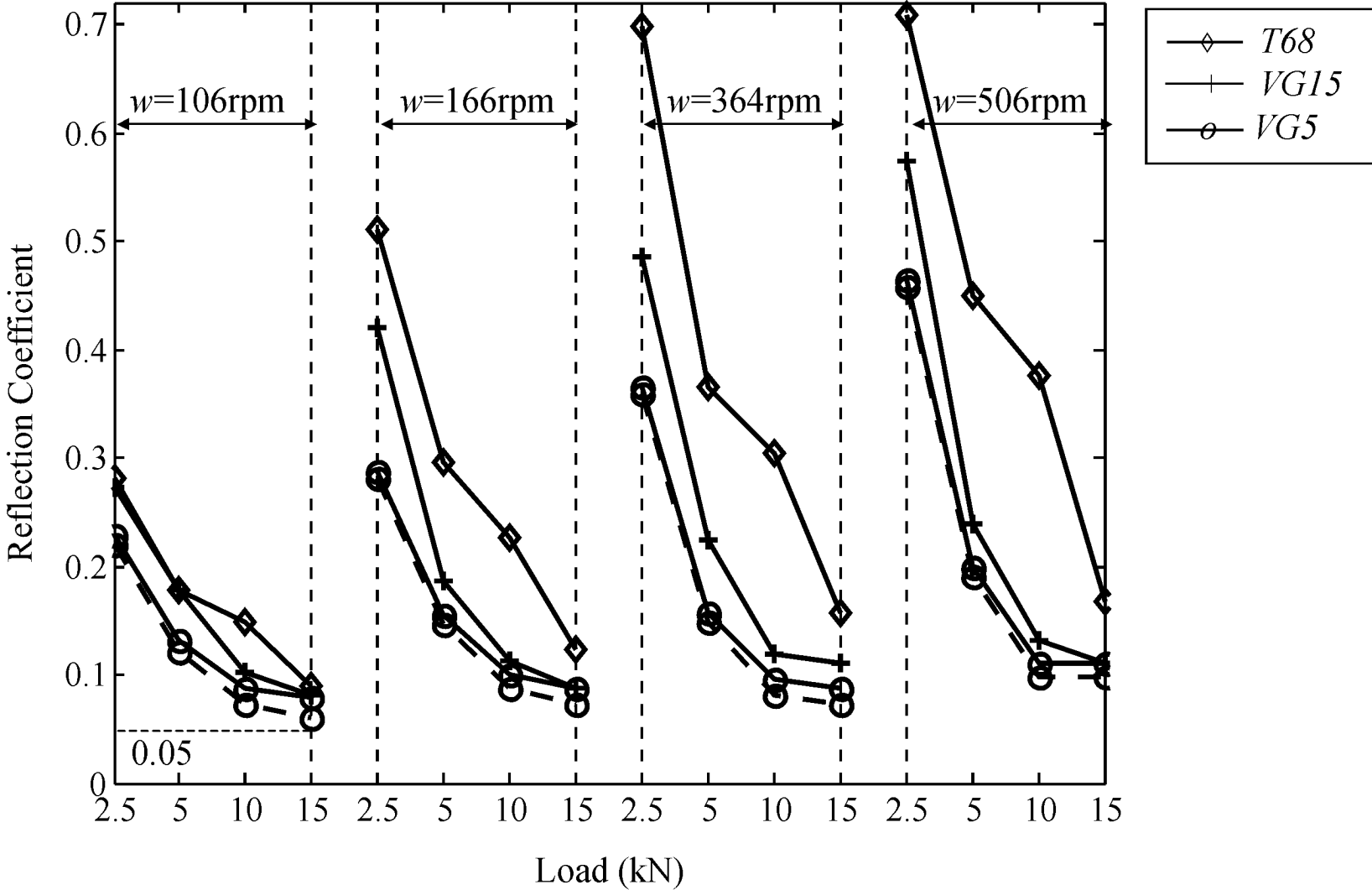


Figure 4.

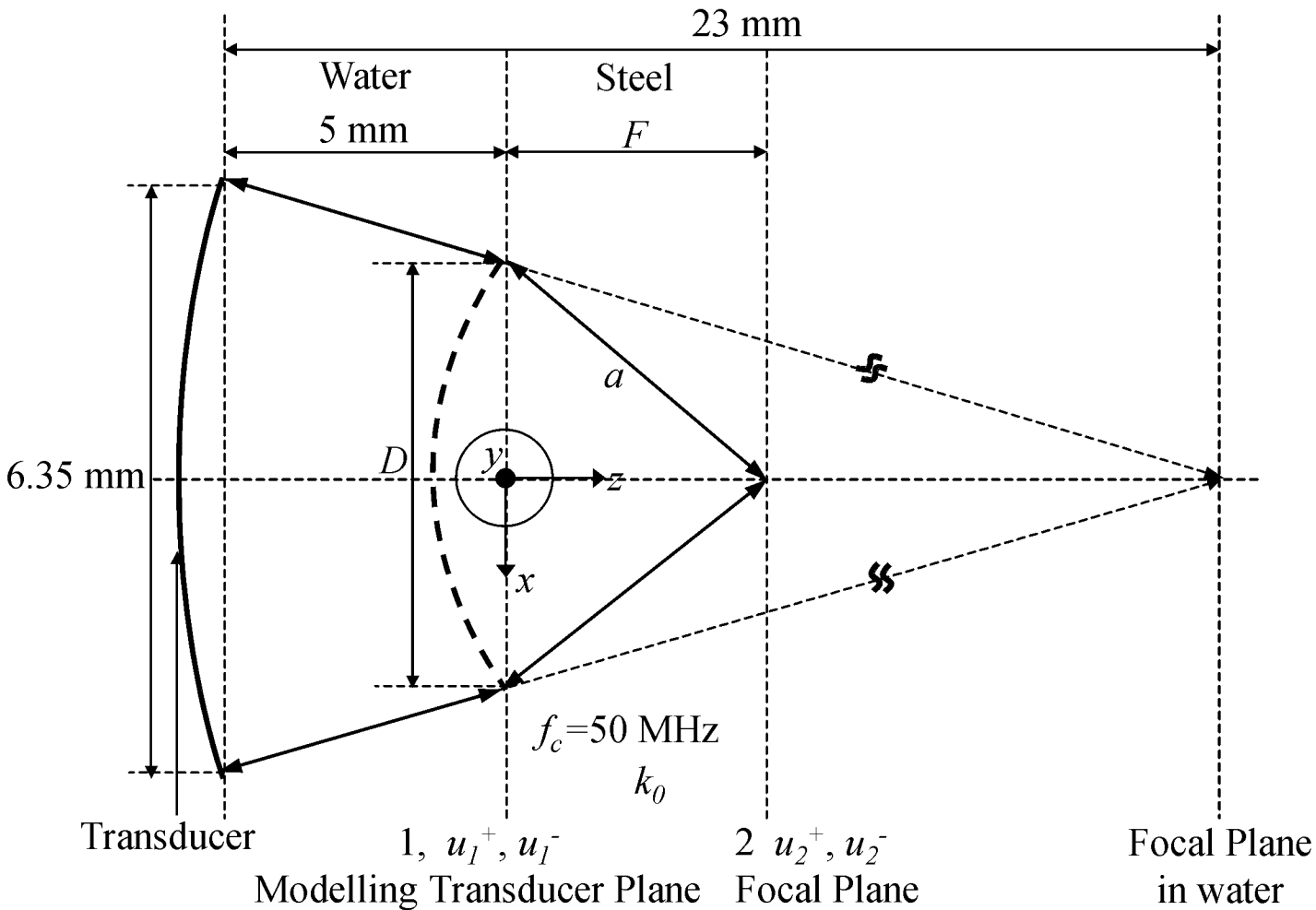


Figure 5.

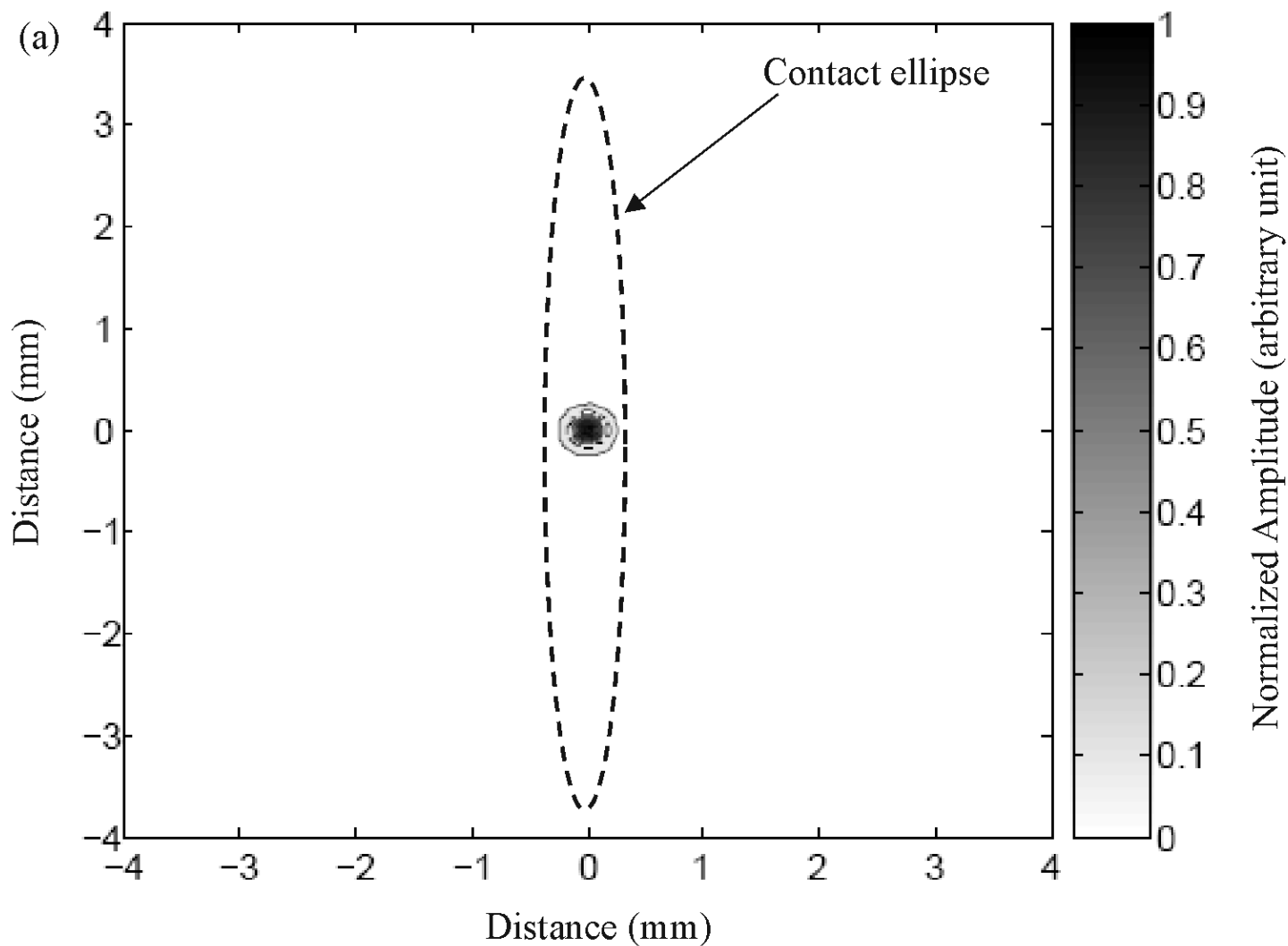


Figure 6(a).

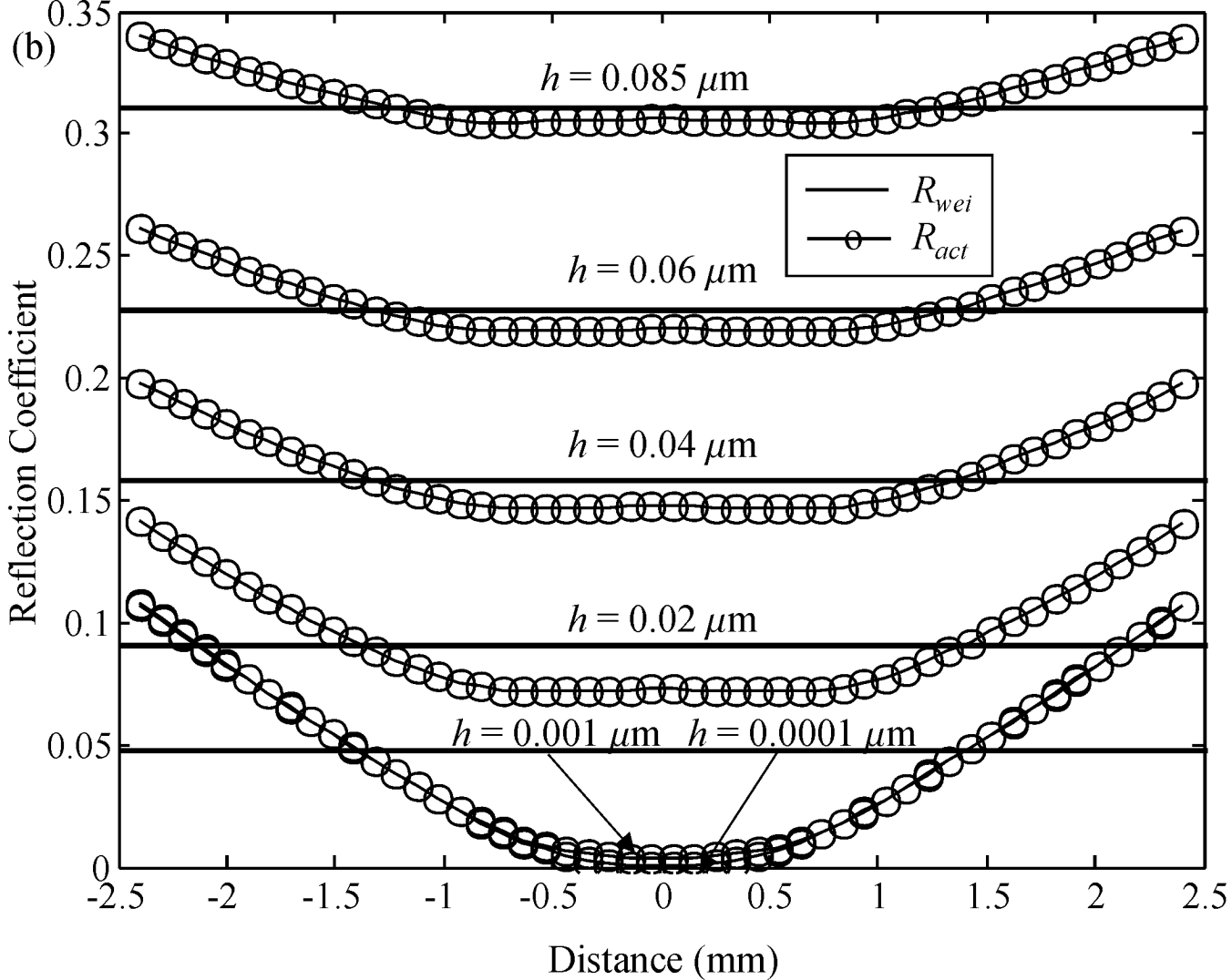


Figure 6(b).

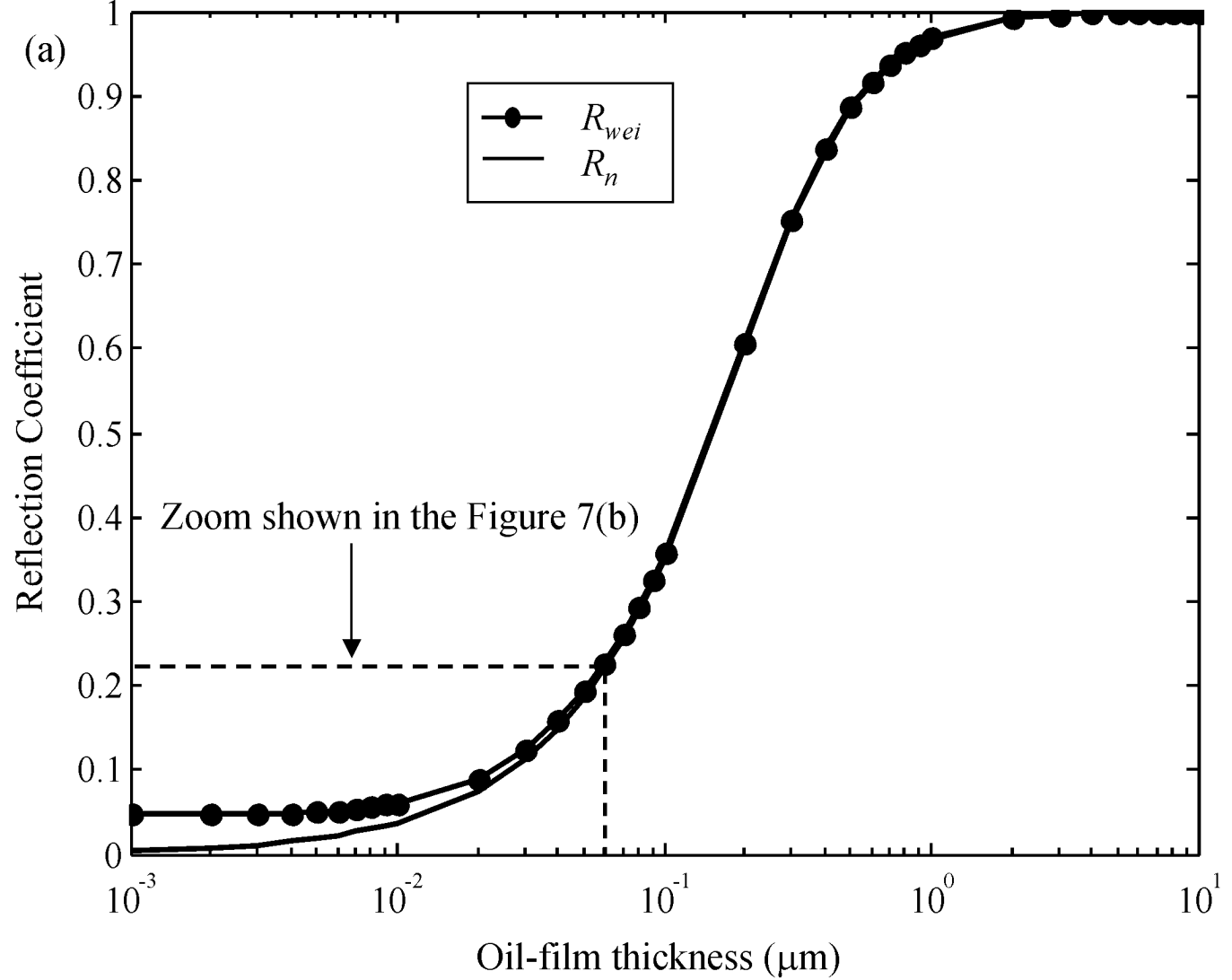


Figure 7(a).

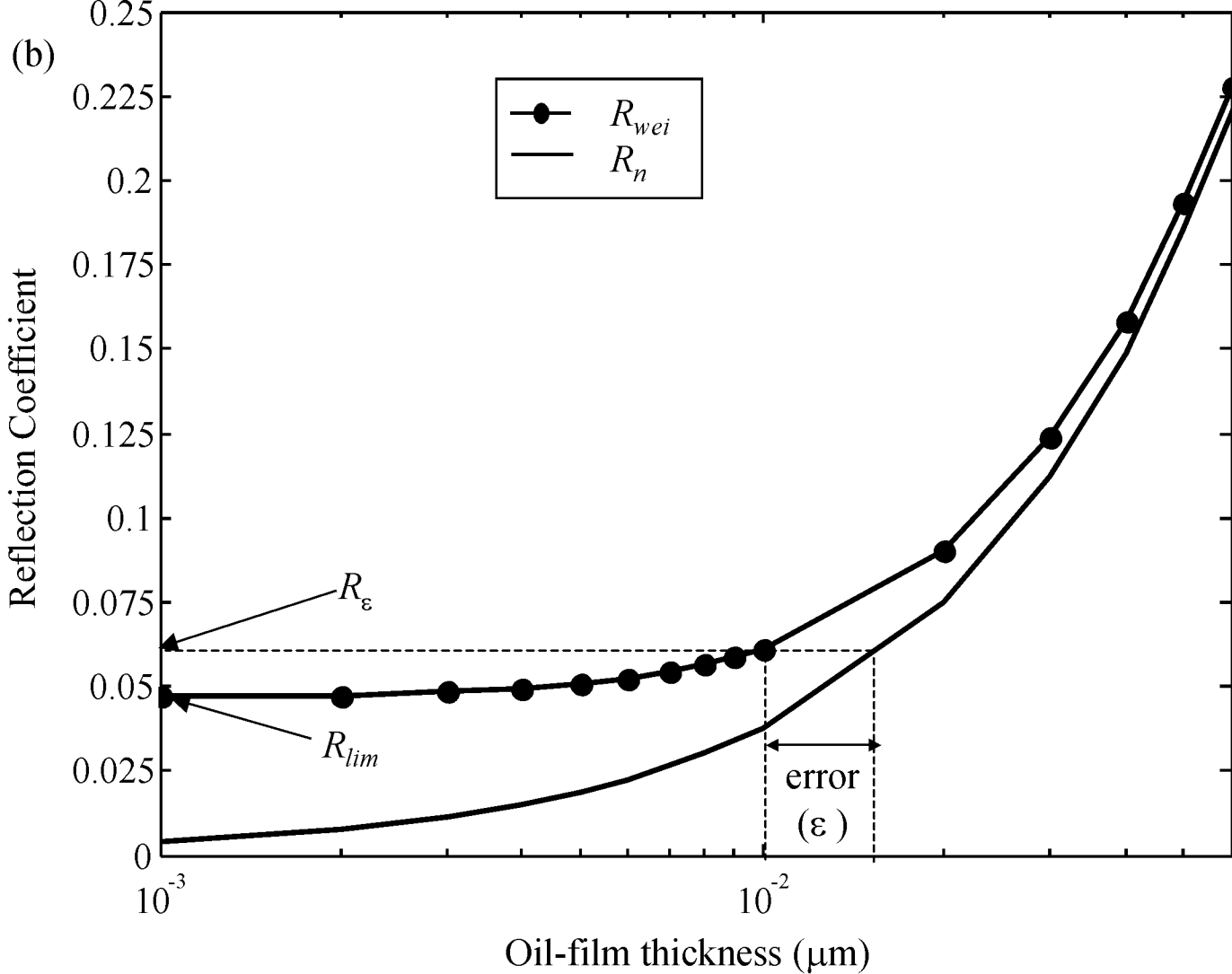


Figure 7(b).

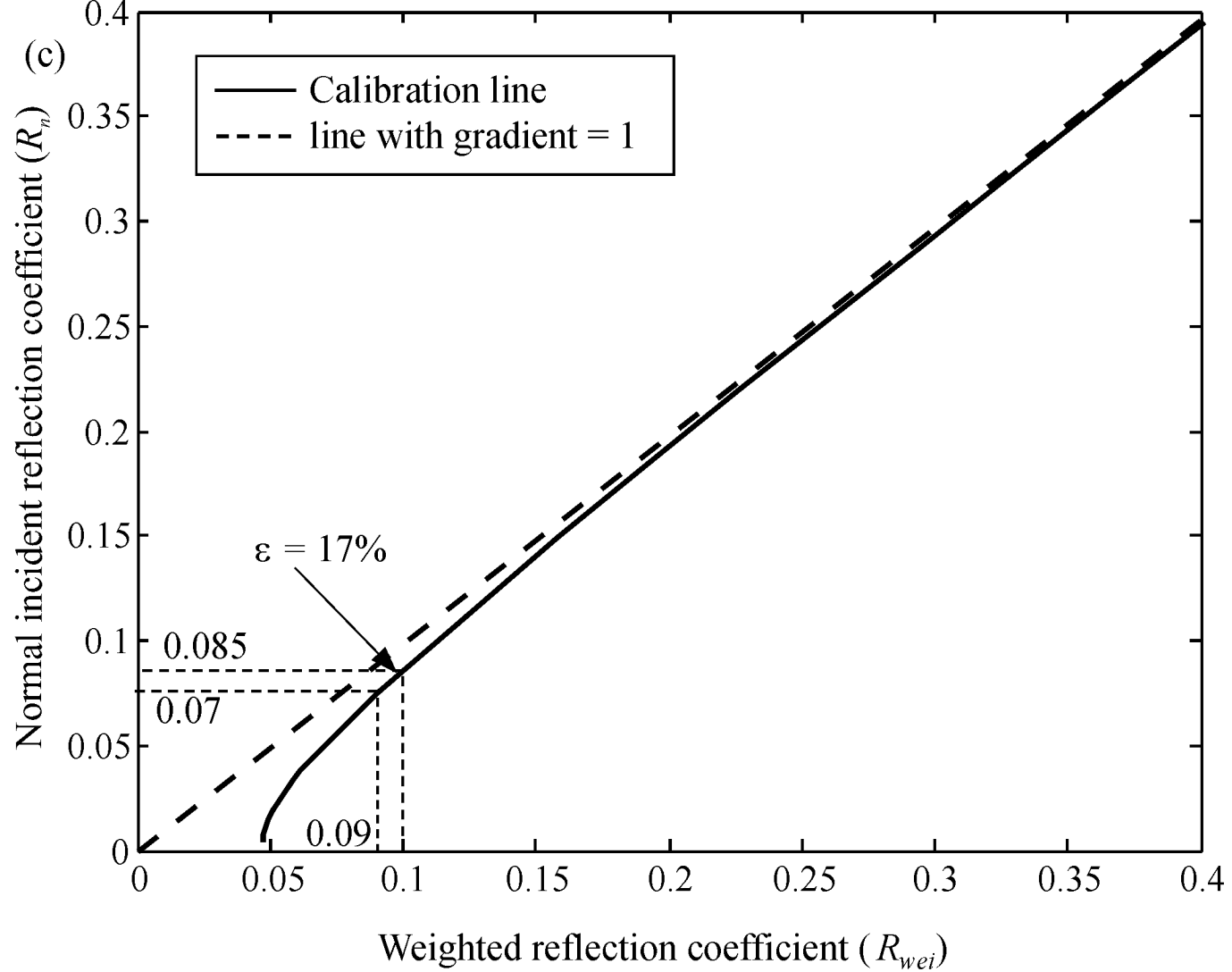


Figure 7(c).

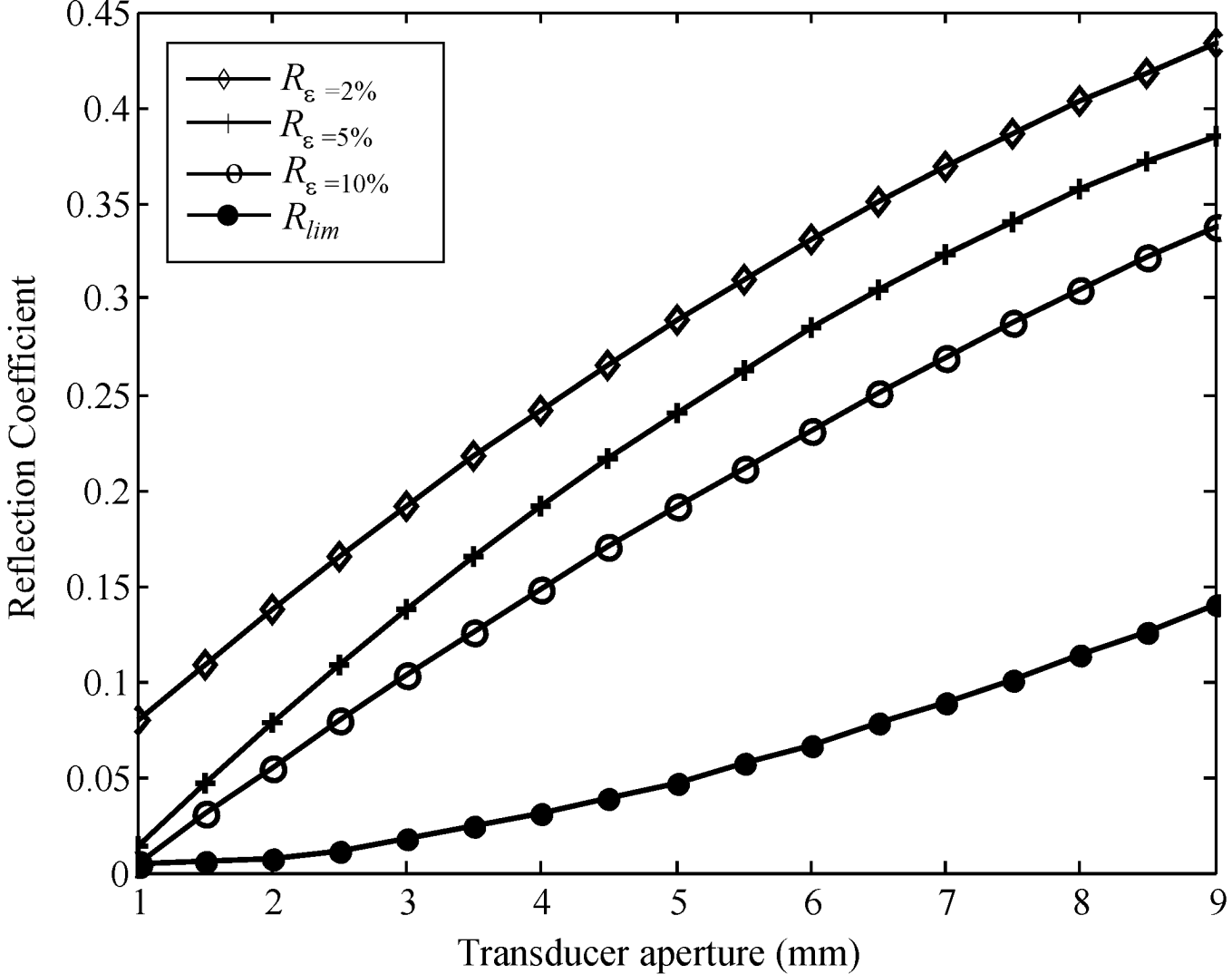


Figure 8.

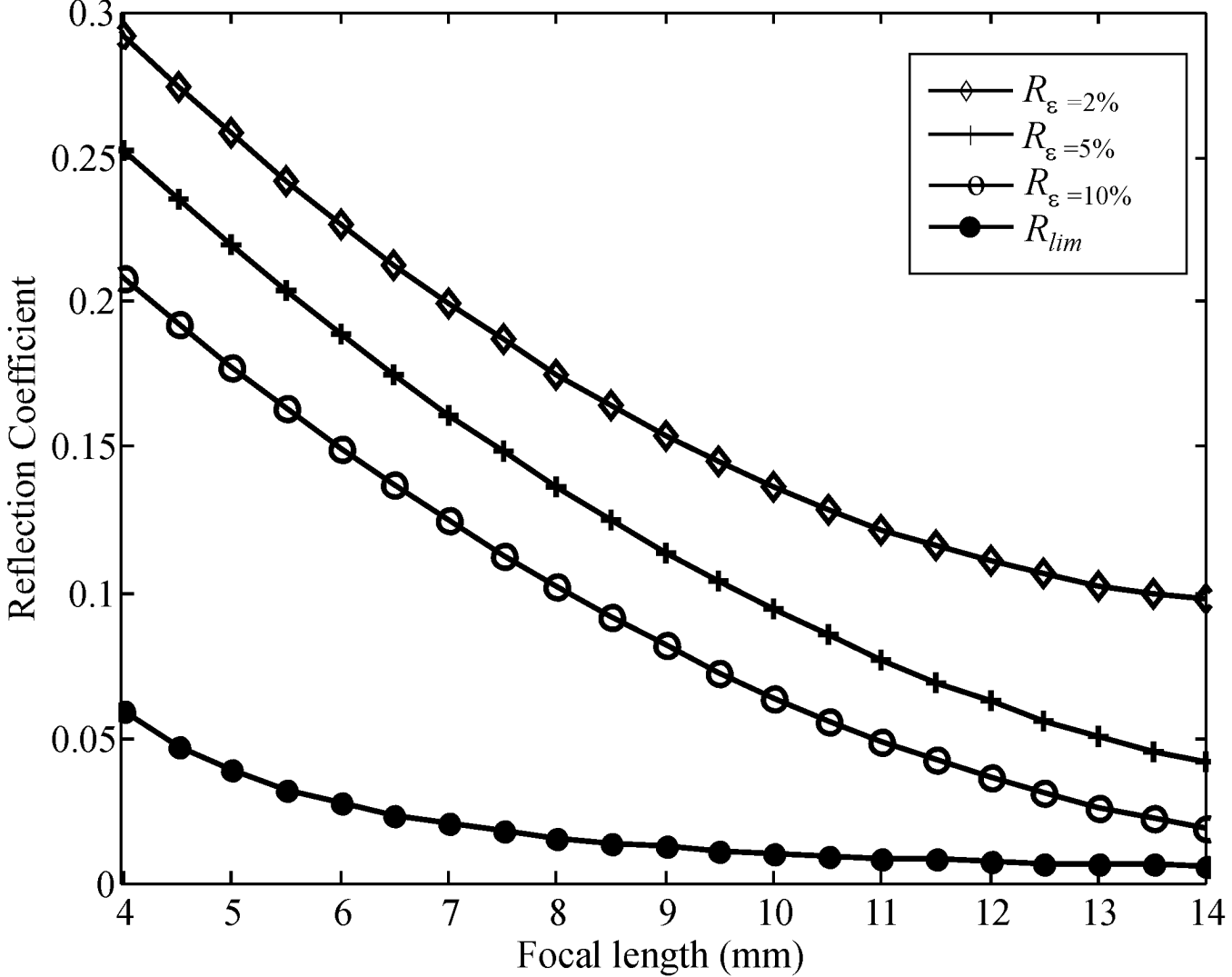


Figure 9.

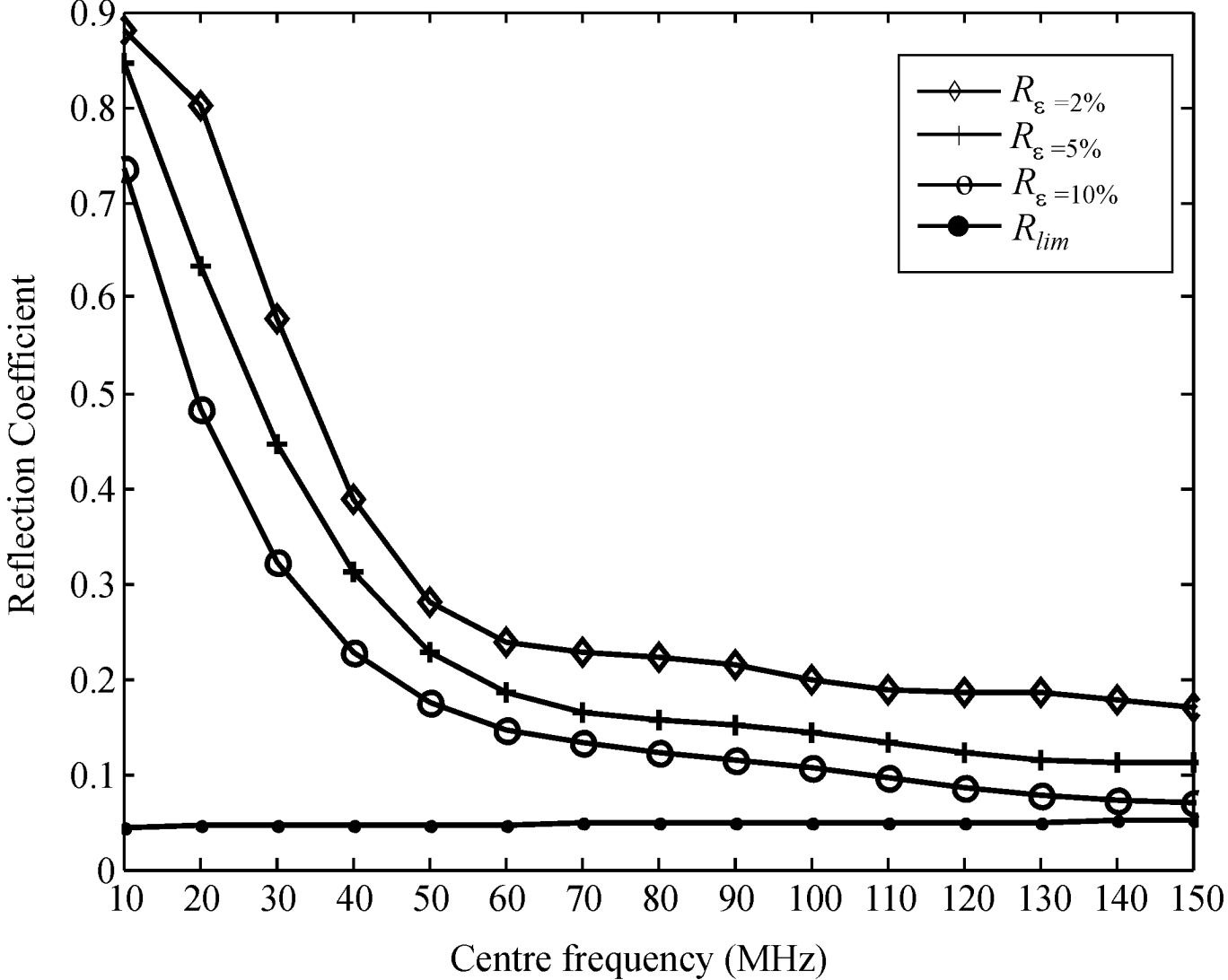


Figure 10.

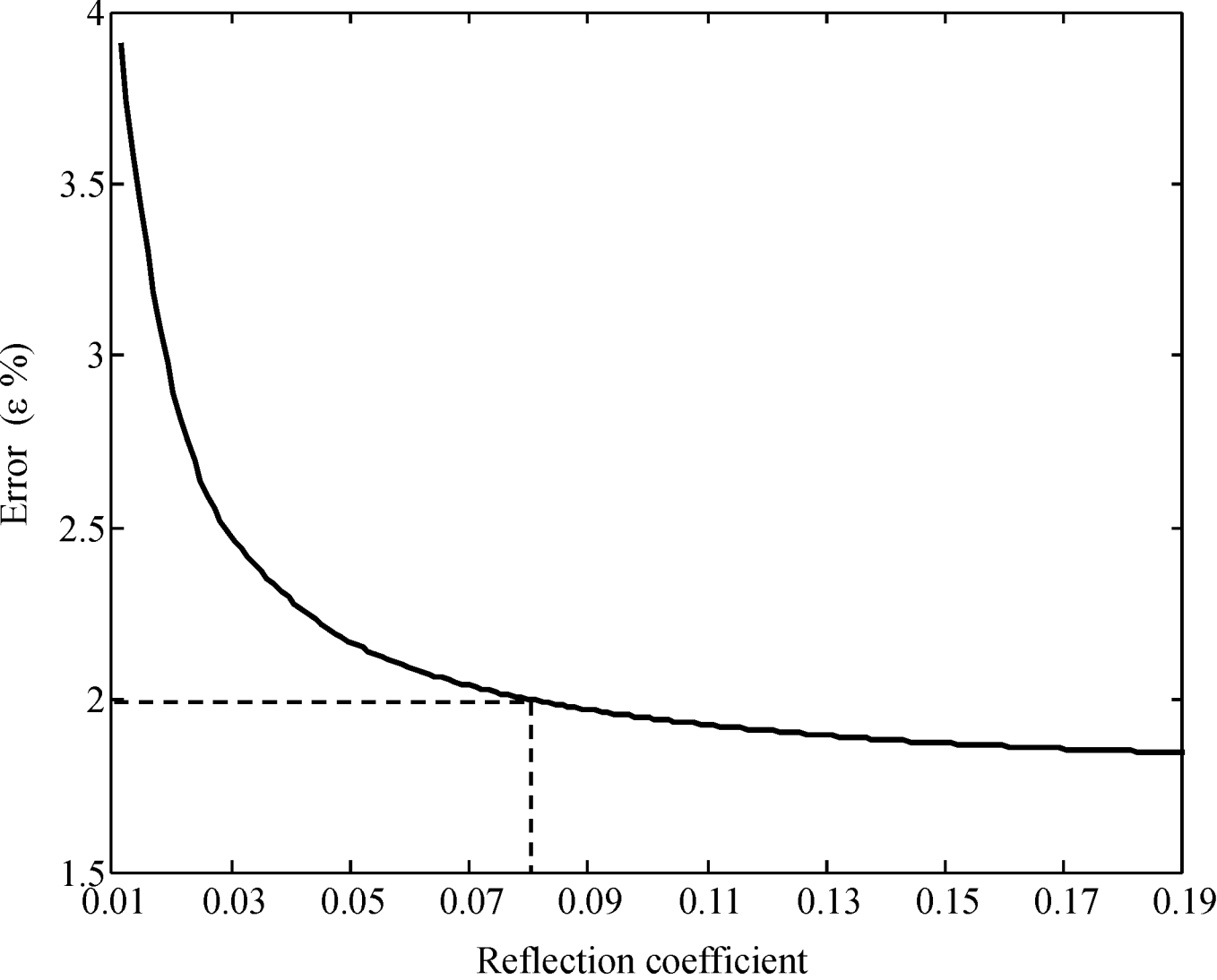


Figure 11.